PNAS RESEARCH ARTICLE | CHEMISTRY

Solvation-induced local structure in liquids probed by high-harmonic spectroscopy

Eric Moore[a], Sucharita Giri[b], Andreas Koutsogiannis[c], Tahereh Alavi[a], Greg McCracken[a], Kenneth Lopata[d], John M. Herbert[c], Mette B. Gaarde[b], and Louis F. DiMauro[a,1]

Affiliations are included on p. 6.

Edited by Angel Rubio, Max-Planck-Institut fur Struktur und Dynamik der Materie, Hamburg, Germany; received June 9, 2025; accepted October 20, 2025

High-harmonic generation (HHG) has been established as a powerful tool for studying structure and dynamics of quantum systems in gas and solid phases. To date, only a few studies have extended HHG spectroscopy to liquids, and much remains unresolved concerning the information that can be extracted from HHG spectra about the local liquid environment and the potential of HHG as a nonlinear probe of solvation dynamics. In this work, we investigate HHG in liquid binary solutions consisting of mixtures of aromatic benzene derivatives solvated in methanol. We observe evidence of a localized solvation structure that is imprinted on the harmonic spectra in the form of a strongly suppressed harmonic order, and an overall reduction of the total harmonic yield. We characterize this behavior as a function of laser parameters, concentration, and other halogenated benzene derivatives in methanol solution. Guided by theory, we interpret the results in terms of a localized solvation shell that is formed in specific solutions and acts like a local scattering barrier in the HHG process. This work demonstrates the potential of high-harmonic spectroscopy in liquids to extract detailed information about the structure and dynamics of solvation while expanding our understanding of the fundamental mechanism of HHG in systems with short-range order.

high harmonic spectroscopy | solute-solvent interactions | ultrafast dynamics | liquids

Significance

Optical linear and nonlinear spectroscopy is the preferred method for studying the interaction between a solute molecule and its surrounding solvent in liquids because photons are minimally intrusive messengers and easily extracted from the solution environment. High-harmonic spectroscopy (HHS) is a new addition to the spectroscopic toolbox that allows exploration in the extreme ultraviolet with time resolution down to the electron's motion. To date, HHS has become a standard probe of electron dynamics, but has been largely confined to gas- and solid-phase studies. Here, we report the results of a study on binary solutions that show the promise of HHS as a nonlinear probe of the structure and dynamics of the local solute-solvent environment.

High-harmonic generation (HHG) can be an exquisite probe of both structure and dynamics in quantum systems and has been widely applied as a time-resolved spectroscopy in gas-phase atoms and molecules, as well as in condensed-phase dielectric crystals and two-dimensional materials (1, 2). In contrast, only a few studies have been performed on HHG in liquid media (3–7) due to the significant challenges involved in both experimental control and theoretical interpretation of the strong-field interaction with liquids. Unlike solids, liquids lack long-range periodicity and unlike gases, the molecules cannot be treated as independent from one another. Instead, liquids exist in a dense, dynamically fluctuating state with only short-range order, creating a complex environment for investigating HHG mechanisms. As a result, relatively little is known about the electron dynamics of strongly driven molecules in the liquid phase, even though many molecules exist most naturally in liquid environments.

Previous studies of HHG in liquids have been performed in pure solvents and have been mainly limited to water and alcohol. The first study of HHG from bulk liquid involved a gravity-fed liquid sheet to compare the harmonic yield of water and heavy water and was limited to low-order harmonics (3). Later, the use of a flat, ultrathin sheet of liquid (4), leading to reduced EUV absorption and phase matching, enabled measurement of HHG spectra from a bulk liquid. More recently, a transition from discrete odd-order harmonics to continuous spectral structure was observed when decreasing the driving pulse duration from multiple cycles to sub-two cycles (6). That study established that the cut-off energy in the liquid phase is independent of pulse duration, in agreement with experiment and ab initio simulation.

In a separate study, Mondal et al. established experimentally the existence of a wavelength-independent cutoff energy in liquid water and liquid alcohol (5). Using a semiclassical model, the authors explained this in terms of a characteristic length scale associated with the elastic-scattering mean free path of electrons in the liquid (8), an interpretation also supported by time-dependent density functional theory (TDDFT) calculations (5, 9). Similarly, several experimental studies have discussed their observed cutoff energies and harmonic yields in terms of electrons scattering on nearby molecules, thereby reducing the cutoff energy and yield [Alexander et al. (10)] or giving rise to a weak, secondary plateau [Mondal et al. (11)]. Previous theoretical studies have used configuration-averaged TDDFT to model the

Author contributions: E.M., G.M., and L.F.D. designed research; E.M., S.G., A.K., T.A., G.M., and J.M.H. performed research; E.M., S.G., A.K., T.A., G.M., K.L., J.M.H., M.B.G., and L.F.D. analyzed data; and E.M., S.G., A.K., M.B.G., and L.F.D. wrote the paper.

The authors declare no competing interest.

This article is a PNAS Direct Submission.

[1]To whom correspondence may be addressed. Email: dimauro.6@osu.edu.

This article contains supporting information online at https://www.pnas.org/lookup/suppl/doi:10.1073/pnas.2514825122/-/DCSupplemental.

Published November 25, 2025.

disordered liquid (5, 9, 11), semiempirical rescattering models incorporating increased scattering on surrounding molecules (5, 10, 11), or introduced random variations of the potential in space in one-dimensional (1D) model calculations (12), obtaining good agreement with the reduced cutoff energies and yields observed experimentally. Other works have introduced defects, dopants, and/or vacancies in 1D models of condensed-phase HHG, and also observed changes in yield and cutoff energy (13, 14).

Nonetheless, many important questions remain about the strong-field/liquid interaction and how to use HHG most efficiently to extract chemically and biologically relevant information. For example, how does the presence of different chemical environments or solvation affect the attosecond electron dynamics, and how is this imprinted on the HHG spectrum?

Here, we explore various liquid environments and the effect of solvation on the HHG process. We present an experimental and theoretical study of HHG spectra in binary solutions consisting of a low concentration of aromatic compounds solvated in methanol. The solute and solvent were chosen to fulfill both fundamental and practical considerations. The halo-benzene derivatives in polar solvents presented an ideal case since they have been extensively investigated in methanol and water with particular emphasis on the fluoro-benzene derivatives, which show significant structural differences in comparison to their non-halogenic counterparts due to the high electronegativity of fluorine (15). Therefore, adjusting the electronegativity of the substituent group by investigating PhF, toluene, and other halogens allowed us to study differences in solvent structure in the context of HHG (Additional discussion is presented in *SI Appendix*). In their pure liquid form, we find that the HHG yield from the aromatic compounds is higher than that of the nonaromatic methanol, in agreement with previous measurements of aromatic versus nonaromatic gas-phase HHG (16). In most of the solutions, we find that the HHG spectrum can be understood in terms of a simple incoherent sum of harmonics generated from the corresponding pure liquids. However, we observe a striking difference in HHG from solutions of fluorinated benzene derivatives in methanol (MeOH), in which the harmonic yield is lower than either of the pure liquids alone. Surprisingly, for fluorobenzene (PhF) in MeOH, we observe almost complete suppression of an individual harmonic order. We find that the photon energy of this harmonic changes between 11.0 and 12.5 eV as we vary the laser intensity and wavelength or the concentration of PhF.

We interpret this result as evidence of local, solvation-induced scattering structure in the PhF–MeOH solution that impedes the HHG process. In the language of the three-step model of HHG (17, 18), tunnel-ionized electrons would scatter off such a structure with a cross-section that depends on kinetic energy, then return to the parent molecular ion with a different phase. We base our interpretations on: i) Molecular dynamics (MD) simulations demonstrating that a new solvation shell is formed around the F atom in PhF–MeOH mixtures, which is not observed in other monohalogenated (Cl, Br, I) benzene derivatives solvated in MeOH. ii) Model calculations solving a 1D time-dependent Schrödinger equation (TDSE) that incorporates a small, local scattering barrier near the ion core, which leads to both overall reduction of the harmonic yield and a strong suppression of a single harmonic, in agreement with the experimental observations. Our experimental results suggest that the HHG process is sensitive to this local structure in the solvation environment, even though the solution as a whole lacks long-range order.

Experimental Results

As a precursor to our studies of HHG in binary solutions, we measured HHG spectra separately in pure MeOH and pure PhX (Ph $\equiv C_6H_5$ and X $\equiv$ F, Cl, Br, I), using driving laser wavelengths of 800 to 3,200 nm, intensities of 20 to 30 TW/cm^2, and pulse durations of 50 to 70 fs. For details about the experimental setup, including the liquid sheet, see *Methods*. For pure liquids, we find that the HHG yields for PhX are stronger than those for MeOH, by 1 to 2 orders of magnitude at fixed intensity, as illustrated in Fig. 1 for PhF (panel *A*) and toluene ($PhCH_3$, panel *B*). Similar differences in harmonic yield have been observed in gas-phase studies when comparing the yield of aromatic versus nonaromatic molecules (16). The aromatic nature of benzene means that π-electron density is delocalized over the carbon ring, leading to a large cross-section that makes PhX derivatives excellent candidates for solutes in MeOH, where their contribution to the HHG process should become apparent even at low concentration (see *SI Appendix* for additional discussion). Consistent with the results in refs. 4 and 5, we also observed wavelength-independent cutoff energies in all of the liquids; see *SI Appendix*, Fig. S3.

Fig. 1 also shows that the HHG spectrum of the solute–solvent mixture differs significantly from each pure-liquid spectrum, but in ways that are unique to each solute. In both cases, the PhF and toluene concentration is low: 9% by mole. In the PhF case, we observe two striking effects in the liquid solution: i) near-total suppression of harmonic 17 (H17) at 12 eV, and ii) an overall decrease in the yield relative to the pure MeOH, even though the pure PhF yield is much higher than that of MeOH. Furthermore, the shape and cutoff energy of the spectrum from the mixture closely resembles that of pure MeOH. In contrast, the harmonics from the toluene–MeOH solution exhibit behavior

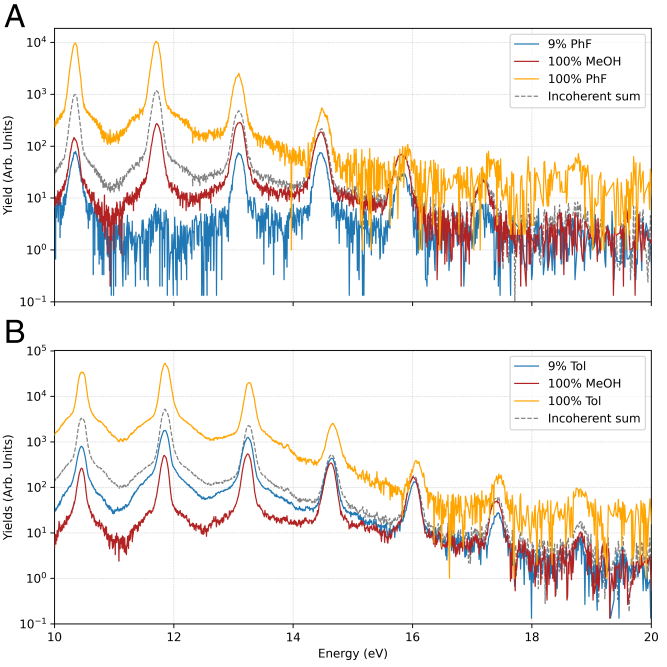

Fig. 1. Harmonic spectra for pure MeOH (orange), pure solute [yellow: PhF in (*A*), toluene in (*B*)], and a solution of 9% solute and 91% MeOH by molar concentration (blue), for a driving laser wavelength of 1,800 nm and an intensity of 30 TW/cm^2. Liquid sheet and laser conditions were identical for all spectra. In both panels, the thin dashed curve shows the incoherent sum of 9% of the PhF yield and 91% of the MeOH yield.

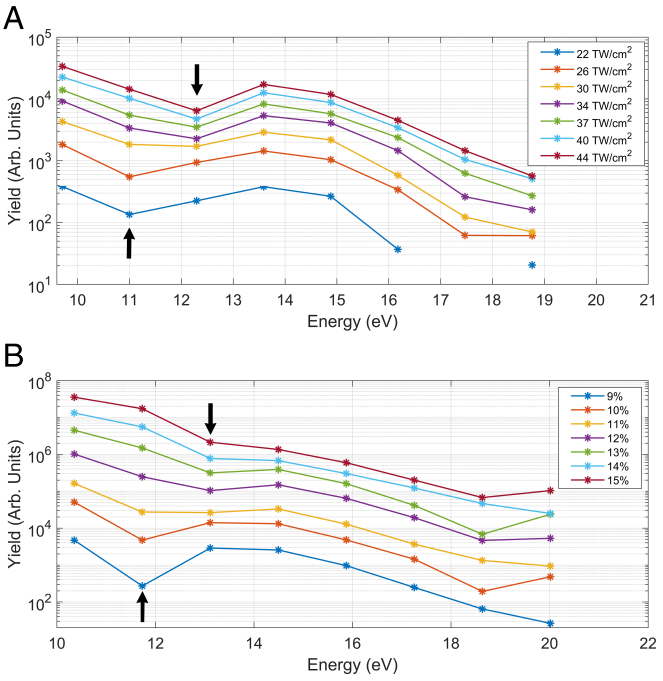

Fig. 2. Integrated harmonic spectra from a PhF–MeOH solution as a function of (*A*) laser intensity for driving wavelength of 1,920 nm, keeping the molar concentrations fixed at 9% PhF and 91% MeOH; or (*B*) molar concentration using 30 TW/cm^2 pulses at 1,800 nm. In all experiments, the sheet conditions used a 425 μL/min flow rate and 3.5 bar of helium pressure. The different curves in (*B*) are vertically offset for clarity. The maximum harmonic suppression is indicated by the black arrows.

more consistent with a simple (incoherent) sum of the harmonic emission from the two individual liquids, resulting in a solution-HHG yield and spectral shape intermediate to the pure liquids. These observations suggest a difference in the HHG process from the PhF–MeOH solution, which drastically deviates from a simple sum of the harmonics emission from constituent liquids, namely a behavior that is indicative of destructive interference. Thus, despite toluene and PhF having similar harmonic yields in their pure forms, their opposing behavior in MeOH solution underscores the significance of solute–solvent interactions. In the following, we explore how this interaction manifests in harmonic spectra as we vary the experimental parameters.

In the experiment, evolution of the harmonic emission is studied by varying laser parameters (intensity and wavelength) and solute concentration. Fig. 2*A* shows the order-integrated HHG amplitude in PhF–MeOH as the intensity is varied while keeping the concentration and wavelength constant, at 9% PhF and 1,920 nm, respectively. As the intensity increases from 22 to 44 TW/cm^2, the suppressed harmonic order continuously evolves from H17 (≈11 eV) at low intensity to H19 (≈12.3 eV) at the highest intensity. Similarly, if we vary the wavelength by keeping the intensity fixed at 22 TW/cm^2, we observe a difference in the depth of the minimum: As we increase the wavelength between 1,700 and 1,840 nm, H17 shifts downward in energy and its suppression deepens until about 1,800 nm (*SI Appendix*, Fig. S4). Next, Fig. 2*B* shows the variation of the HHG spectra as the PhF concentration varies from 9% to 14%, with the laser intensity and wavelength fixed at 30 TW/cm^2 and 1,800 nm, respectively. The figure shows that the energy of the suppressed harmonic steadily increases with PhF concentration, from below 12 eV to above 13 eV, and that the minimum becomes more shallow.

As documented above, the single-harmonic suppression is robust for HHG in PhF–MeOH solution across varying wavelengths, intensities, and concentrations. To explore whether this behavior is specific to fluorinated benzene derivatives, we studied other halobenzenes (PhCl, PhBr, and PhI) under similar conditions and concentrations. Fig. 3 presents the results, showing the harmonic yields and their ratios relative to the pure MeOH yield. These results clearly show that the harmonic yield suppression in the PhF–MeOH solution is unique; all other halobenzene solutions exhibit an *enhancement* of the yield in the 10 to 14 eV range, similar to behavior observed in the toluene–MeOH solution. The enhancement increases with the halogen's molecular weight, ranging from 4× for PhCl, and 13× for PhBr and PhI. The behavior of all three solutions is much closer to what one would expect for a simple mixture of two noninteracting species, suggesting a lack of strong solute–solvent interactions. In the following, we explore the origin of the unique spectral suppression of HHG in the PhF–MeOH solution.

Interpretation and Theoretical Modeling

We propose that the observed HHG behavior of the PhF–MeOH solution can be understood in terms of a local solvation-induced scattering structure that impedes the generation of harmonics from MeOH in the presence of a low concentration of PhF. Such a feature could be either static or dynamic, i.e., stemming either from the inherent structure of the liquid solution or else induced by the strong laser field, or some combination thereof. In the language of the three-step model of HHG (17, 18), electrons ejected from MeOH would scatter off of the local, solvation-induced structure with a cross-section depending on kinetic energy, returning to the parent molecular ion with a different phase. Low kinetic energy electrons near their classical turning point have the highest cross-section and are most likely to scatter, so that a spatially localized structure could lead to destructive interference of the harmonic emitted upon return of those electrons. This model would also explain the overall decreased HHG yield for the PhF–MeOH solution compared to pure MeOH, as the solvation structure introduced by the presence of PhF disturbs the generation of all the harmonics, not simply the single harmonic that is completely suppressed.

Fig. 4*A* illustrates how the maximum excursion of an electron (within the three-step model) is related to the emitted harmonic energy upon return, for a laser wavelength of 1,920 nm and two different laser intensities, 22 and 44 TW/cm^2. The shaded blue "barrier" at the bottom is illustrative of a narrow solvation structure located at some distance from the core, taken here to be 3 Å. As the intensity is increased, the trajectory sampling a 3 Å distance with near-zero energy corresponds to a return energy (photon energy) shifted by one harmonic order, i.e., H17 → H19. This is consistent with the intensity-dependent behavior we observed in Fig. 2*A*, in which the suppressed harmonic shifted to higher energy as the laser intensity was increased. It is also consistent with our observed wavelength dependence: A scattering barrier at a fixed distance would lead to a small (<0.2 eV) downward shift of the maximally suppressed return energy over the wavelength range 1,700 to 1,840 nm. This would mean that the photon energy of H17 would move from being slightly above to almost coincident with the maximally suppressed energy.

We explore a potential structural origin of such a scattering barrier by investigating the average structure of PhX–MeOH solutions using classical MD simulations (19, 20), as described

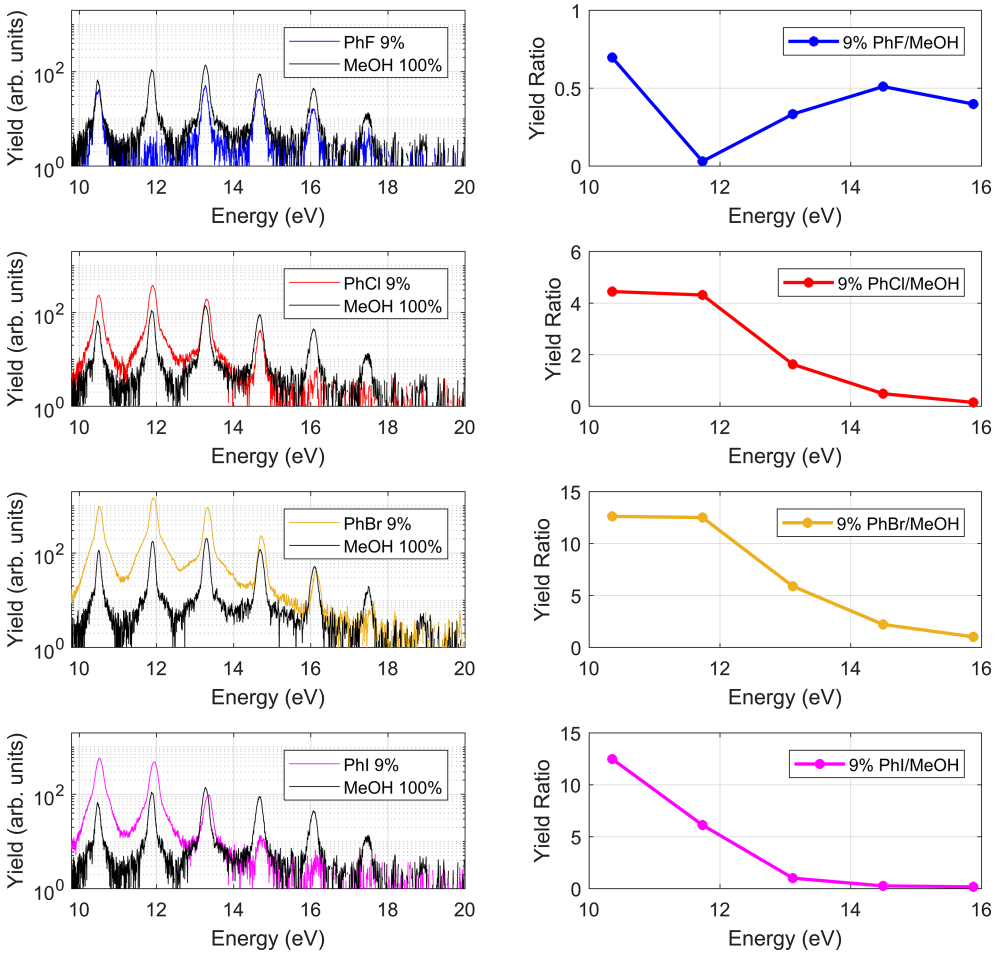

Fig. 3. *Left* side: Harmonic spectra for different PhX–MeOH solutions (at 9% mole concentration) compared to those of pure liquid MeOH. *Right* side: ratio of HHG yield in solution versus pure MeOH. In all cases, the laser intensity and wavelength are 30 TW/cm^2 and 1,800 nm, respectively.

in *Methods*. We equilibrate a 9% solution of PhF in MeOH at a normal liquid density of 0.8341 g/cm^3 and room temperature and then use it to calculate radial distribution functions (RDFs) for hydroxyl hydrogen atoms from MeOH around the halogen atom in PhX, as shown in Fig. 5. The small structure near 2 Å, which is exclusive to the fluorine case, is indicative of a solute–solvent hydrogen bond. Integration of the RDF up to the first local minimum suggests that a 9% solution of PhF has about nine PhF$\cdots$HOCH$_3$ hydrogen bonds per 100 solvent molecules, which means that every PhF molecule is involved in forming a bond. It is a minor feature because the PhF solute mostly occupies voids that are known to exist in the structure of liquid MeOH (21, 22), but it is entirely absent except for PhF where the PhF$\cdots$HOCH$_3$ interaction strength is largest. As compared to fluorine, hydrogen bonding is much less directional in larger halides, due to the decreased interaction strength (23).

Thus, one possible cause for the strong suppression of the harmonic yield in PhF–MeOH solution, as compared to solutions of the other halobenzene derivatives, could be the extra solvation shell formed by the PhF$\cdots$HOCH$_3$ bonds. The high electronegativity of the F atoms would cause an increased electron density in the vicinity of the affected MeOH molecules, forming a scattering barrier as discussed above. Although the $\approx$2 Å distance in the RDF is smaller than the characteristic distance considered for the repulsive barrier illustrated in Fig. 4*A*, the center of the MeOH molecule is separated from the F atom by another 1 to 2 Å. This suggests that HHG in liquids can potentially be sensitive to the local spatial and temporal structure of the solvation environment, perhaps even extending to identifying the most likely ionization and recombination sites; see also ref. 11.

We next illustrate the electron-scattering-based suppression discussed above with a simple 1D solution of the TDSE that incorporates a scattering barrier located a few Å from the ion core. We calculate the HHG spectrum using a model that treats a liquid-phase MeOH molecule by a soft Coulomb potential. The potential is altered in two ways: i) the softening parameter is adjusted to match the ionization potential of liquid-phase MeOH (9.8 eV), and ii) we incorporate the overall effect of the reduced mean free path of the liquid environment through an absorbing boundary beginning around 8 Å from the core. This placement of the absorbing boundary lowers the cutoff energy to below 20 eV, consistent with the experimental observation, and also generally consistent with the findings of Mondal et al., that the effective maximum excursion distance in the liquid is much lower than in the gas phase (5). To introduce a local scattering structure near the molecule, we add a small repulsive potential barrier to the soft Coulomb potential, centered at distance x_0 from the core, and with a height and full width at half maximum (FWHM) of 3.6 eV and 1.1 Å, respectively. For more details about the TDSE calculations and the barrier size and shape, see *Methods*.

The *Inset* of Fig. 4*B* displays HHG spectra driven by 1,800 nm, 20 TW/cm^2 pulses for two different locations of the repulsive

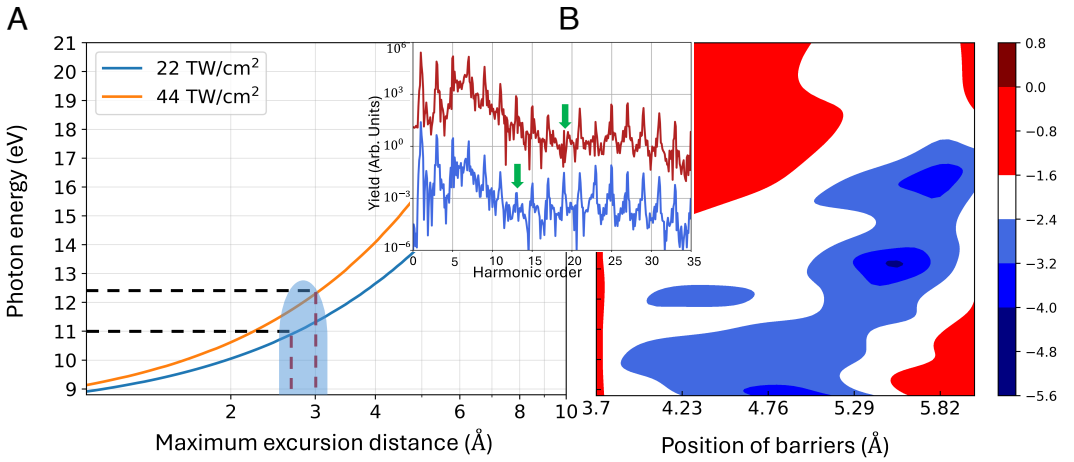

Fig. 4. (*A*) Semiclassical prediction for the emitted photon energy versus maximum excursion distance, for 1,920 nm light with two different intensities. The blue shading represents the position of a local scattering structure. The dashed black lines mark the coincidence of the H17 and H19 turning point with the barrier. (*B*) 2D plot of harmonic yield (calculated from the TDSE) versus position of the local barrier, normalized to the yield in the absence of the barrier, for a 20 TW/cm^2, 1,800 nm laser pulse. Yields have been calculated from a single cycle of the field to smooth out individual harmonic peaks. The *Inset* shows individual spectra for two different positions of the barrier, $x_0 = 4.65$ Å (blue) and 5.50 Å (red).

barrier. The spectra are vertically offset for clarity. The dipole spectrum is calculated using a trapezoidal flat-top laser pulse and shows a sharp suppression of individual harmonic orders that shifts to higher photon energy as the barrier distance from the core is increased. This supports our interpretation based on the rescattering model discussed above: that a spatially localized structure near a molecule can lead to suppression of a single harmonic, consistent with the experimental observation in the PhF–MeOH solution spectra.

The suppression is illustrated more systematically in Fig. 4*B*, which shows a 2D map of the harmonic spectrum versus the barrier location, normalized by the spectral yield in the absence of the barrier. Here, we have calculated the spectral yield from a single burst of harmonic radiation in order to show the smooth variation of the minimum yield. The blue regions in the map signify a sharp suppression of harmonics caused by the barrier, and show that the suppression shifts to higher energy and slowly broadens as the barrier moves outward, in agreement with the spectra shown in the *Inset*. In addition, we note that the barrier suppresses the harmonic yield over a broad range of harmonics, also in agreement with experimental observations in the PhF–MeOH case. A time-frequency analysis of the dipole radiation shows that the overall suppression happens because the barrier reduces the return probability for all the short-trajectory electrons, without otherwise altering their behavior significantly. In addition, scattering on the barrier facilitates a weaker family of trajectories that return almost a half cycle later and cause sharp destructive interference for a narrow range of return energies. For more details, see *SI Appendix*, Fig. S7. While the extra repulsive potential has some similarity to that supporting a shape resonance in terms of its location (24), it is much weaker and functions predominantly as a scattering barrier rather than supporting additional bound states in the continuum.

It is clear that a 1D single-active-electron model cannot capture the complex many-electron dynamics involved in a solvated system interacting with a strong laser pulse. However, in combination with the MD simulation results it nevertheless supports our hypothesis that a local structure is formed in the PhF–MeOH solution, which leads to additional scattering and which is absent in the other solutions. In principle, such a structure could either be inherent to the solvation environment itself, or it might form in the presence of the strong field. It is also possible that the strong laser field enhances or otherwise interacts with the local order along its polarization direction or that it induces a dynamical structure, which may modify the inherent liquid structure of the PhF–MeOH solution. Interestingly, MD simulations for a 14% solution of PhF in 85% MeOH do not show any significant change in the position of the PhF...HOCH3 hydrogen bond relative to the 9% solution (*SI Appendix*, Fig. S8). This is not unexpected, but it implies that the structure of the two liquids differs in subtle ways that are difficult to capture in the RDF. It also again emphasizes the exquisite sensitivity of high-harmonic spectroscopy enabled by the coherent nature of the generation process.

Experimentally, we have also observed the disruptive behavior of difluorinated compounds $C_6H_4F_2$ at 9% molar concentration in MeOH, which similarly results in overall suppression of the harmonic yield compared to both pure methanol and pure $C_6H_4F_2$ (*SI Appendix*, Fig. S5). In these solutions, we do not

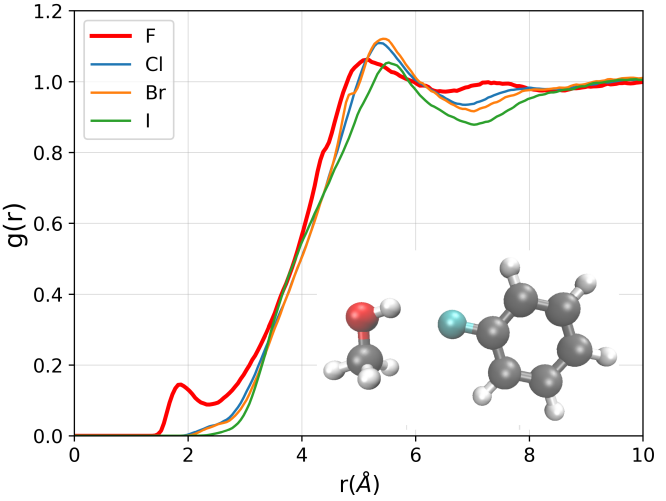

Fig. 5. Site–site (halogen to hydroxyl hydrogen) RDF for a 9% (by mole) PhX solution in 91% MeOH, with X = F, Cl, Br, or I. The small peak near 2 Å for PhF–MeOH is indicative of a $CH_3OH\cdots FC_6H_5$ hydrogen bond, as suggested by the *Inset* figure.

observe suppression of individual harmonic yields nor do we see evidence of a new solvation structure around the fluorine atoms in MD simulations for $C_6H_4F_2$ in MeOH. Finally, we note that Chandra and collaborators (25) observed an influence of hydrogen bonding on the yield of HHG radiation in joint experiment-theory work, in the mixture of two gases that are likely to form hydrogen bonds. They suggested that the delocalized electron density associated with the hydrogen bond may enhance the harmonic yield, similar to that observed from the aromatic versus nonaromatic molecules (16).

Conclusions

We have explored HHG from binary solutions of benzene derivatives in MeOH. We observed unique features in the HHG spectrum from the solution of fluorinated derivatives, which we attribute to solute–solvent interactions in the formation of the liquid and/or in its interaction with the strong laser field. In particular, we interpret the robust, near-complete suppression of a single harmonic in terms of a local solvation structure that is formed in the PhF–MeOH mixture and acts as a scattering barrier for near-zero kinetic energy electrons during the HHG process. We hypothesize that hydrogen bonding of PhF to MeOH, unique among halobenzene derivatives, may perturb the MeOH solvation shell and provide the scattering barrier leading to the observed harmonic suppression. These results demonstrate that solution-phase HHG can be sensitive to features of the solute–solvent interaction, and thus to the local liquid environment. They serve to increase our understanding of attosecond dynamics in chemically and biologically relevant liquid-phase systems. It is worth noting that the rescattering electrons involved in the HHG processes have low energy (a few eV or less). Collision and scattering processes of low energy electrons in liquid environments can play important roles in radiation damage in organic tissue in the form of solvated electrons (26) and DNA strand breaks (27–29).

Methods

Experimental Setup. Most experiments used 1,200 to 2,400 nm pulses with 70 fs duration generated in a commercial optical parametric amplifier (OPA) HE-TOPAS Prime (Light Conversion) pumped with a Ti:Sapphire laser system (Spitfire Ace by Spectra Physics). The infrared pulses are focused with a 30 cm focal length AR coated lens onto an ultrathin liquid sheet in a vacuum environment. The emitted harmonic light is collected by a VUV spectrometer. An overview of the experimental apparatus is depicted in *SI Appendix*, Fig. S1.

Specifically, the liquid sheet is formed using a gas-accelerated microfluidic nozzle (Micronit Technologies) (30). This method produces ultrathin liquid sheets with a thickness of <100 nm. The liquid samples were pumped with a high-performance liquid chromatography pump (Shimadzu LC-20AD) and circulated into the vacuum chamber through PEEK tubing. The velocity of the liquid exiting the nozzle is typically around 4 to 5 m/s. Consequently, every laser shot (with a spot size around 70 μm and 1 kHz repetition rate) interacts with a newly replenished sample. The sheet is characterized by thickness and position. The sheet thickness is measured in situ using an interferometric approach (precision ±16 nm) that incorporates an 800 nm *cw*-laser diode and binary 0–π phase grating. Positioning is continuously monitored using a high spatial resolution optical imaging system.

The harmonic detection system uses an easyLight VUV spectrometer (HP Spectroscopy) designed to measure the spectral range of 30 to 250 nm (5 to 40 eV). The dispersed harmonic light was collected on a microchannel plate chevron with a phosphor screen and subsequently imaged on a CMOS camera. The intensity at the laser focus was calculated geometrically from the measured spot size and power calibration before each experiment and verified with the harmonic cutoff energy from gas harmonics.

HHG Model Calculations. We illustrate the effect of a local solvation structure in the liquid environment by solving a 1D TDSE incorporating a small scattering barrier. The liquid environment is simulated by first adjusting the softening parameter of the soft-core Coulomb potential to obtain the ionization potential of liquid MeOH (9.8 eV). Second, we incorporate the overall effect of the reduced mean free path of the liquid environment through an absorbing boundary that starts at 8 Å from the core and slowly suppresses the wavefunction over 32 Å to avoid artificial reflections from the boundary. Finally, the effect of a local scattering structure near the emitter is modeled by adding a small repulsive component to the potential. The repulsive potential is a Gaussian (everything is in atomic units), given by

$$V(x) = \frac{\exp[(x - x_0)^2/2\sigma^2]}{N\sqrt{2\pi}},$$

where x_0 represents the central position of the potential with respect to the soft-core Coulomb center, N controls the height (strength) of the barrier and σ denotes its width. The HHG spectra and 2D color map in Fig. 4*B* are plotted for a barrier whose height and FWHM are 3.6 eV and 1.12 Å (N = 3.0 and σ = 0.9 a.u.). The impact of this repulsive potential barrier on the HHG process is analyzed by varying the parameters N, σ, and x_0, allowing us to study how changes in the height, width, and central position of the barrier influence the HHG calculation. To analyze the cumulative effect of neighboring atoms at various distances, we consider the coherent contributions of five consecutive barriers. These multiple contributions also serve as an averaging or smoothing function: Each single barrier generally suppresses a specific harmonic, though the degree of suppression is more sensitive to differences in laser and potential parameters.

For specific parameters of the repulsive barrier, we observe that suppression of a particular harmonic in the HHG spectra can occur. By fixing the central position of the barrier and varying the height and width across a wide range, we observed that this suppression is strongly correlated with the position of the barrier and is much less sensitive to its height and width. This is illustrated in *SI Appendix*, Fig. S6. Suppression of the specific harmonic does not depend on the exact placement and shape of the absorbing boundary potential.

MD Simulations. Classical MD simulations were performed in the canonical (*NVT*) ensemble using the Tinker-HP program (19) and the OPLS-AA force field (20). A 9% solution of PhX (by mole) in MeOH, at normal liquid density (ρ = 0.8341 g/cm^3), was equilibrated for 3 ns at a target temperature T = 298 K, in a cubic simulation cell with L = 34.557 Å under periodic boundary conditions. A Berendsen thermostat with τ = 0.1 ps was used to regulate the temperature. Snapshots were collected at every 0.5 ps of a subsequent 7 ns production run. A similar procedure was followed for a 14% solution, using L = 35.898 Å to achieve the same density. A comparison between the 9% and the 14% solution of PhX in MeOH is shown in *SI Appendix*, Fig. S8.

Data, Materials, and Software Availability. Code data have been deposited in GitHub (https://github.com/girisucharita/1D_tdse_model.git). All other data are included in the manuscript and/or *SI Appendix*. Processed data, codes, and scripts are available in a public repository (31).

ACKNOWLEDGMENTS. E.M. and L.F.D. acknowledge the technical guidance on the microfluid jet by Dr. Daniel DePonte (SLAC). Work at The Ohio State University was supported by the U.S. Department of Energy, Office of Science, Basic Energy Sciences, under Awards DE-FG02-04ER15614 and DE-SC0012462, except that A.K. and J.M.H. were supported by NSF grants CHE-1955282 and CHE-2402361. Work at Louisiana State University was supported by the U.S. Department of Energy, Office of Science, Basic Energy Sciences, under Award DE-SC0012462.

Author affiliations: [a]Department of Physics, The Ohio State University, Columbus, OH 43210; [b]Department of Physics and Astronomy, Louisiana State University, Baton Rouge, LA 70803; [c]Department of Chemistry and Biochemistry, The Ohio State University, Columbus, OH 43210; and [d]Department of Chemistry, Louisiana State University, Baton Rouge, LA 70803

1. F. Krausz, M. Ivanov, Attosecond physics. *Rev. Mod. Phys.* **81**, 163 (2009).
2. S. Ghimire, D. A. Reis, High-harmonic generation from solids. *Nat. Phys.* **15**, 10–16 (2019).
3. A. D. DiChiara, E. Sistrunk, T. A. Miller, P. Agostini, L. F. DiMauro, An investigation of harmonic generation in liquid media with a mid-infrared laser. *Opt. Express* **17**, 20959–20965 (2009).
4. T. T. Luu *et al*., Extreme-ultraviolet high-harmonic generation in liquids. *Nat. Commun.* **9**, 3723 (2018).
5. A. Mondal *et al*., High-harmonic spectroscopy of low-energy electron-scattering dynamics in liquids. *Nat. Phys.* **19**, 1813–1820 (2023).
6. A. Mondal *et al*., High-harmonic generation in liquids with few-cycle pulses: Effect of laser-pulse duration on the cut-off energy. *Opt. Express* **31**, 34348–34361 (2023).
7. J. Xu, S. Meng, High-harmonic generation and femtosecond-resolved ultrafast dynamics in liquid water. *J. Phys. Chem. Lett.* **16**, 5295–5301 (2025).
8. T. Gadeyne, P. Zhang, A. Schild, H. J. Wörner, Low-energy electron distributions from the photoionization of liquid water: A sensitive test of electron mean free paths. *Chem. Sci.* **13**, 1675–1692 (2022).
9. O. Neufeld, Z. Nourbakhsh, N. Tancogne-Dejean, A. Rubio, Ab initio cluster approach for high harmonic generation in liquids. *J. Chem. Theory Comput.* **18**, 4117–4126 (2022).
10. O. Alexander *et al*., Observation of recollision-based high-harmonic generation in liquid isopropanol and the role of electron scattering. *Phys. Rev. Res.* **5**, 043030 (2023).
11. A. Mondal *et al*., Multi-plateau high-harmonic generation in liquids driven by off-site recombination. arXiv [Preprint] (2025). http://arxiv.org/abs/2506.23945 (Accessed 30 June 2025).
12. A. W. Zeng, X. B. Bian, Impact of statistical fluctuations on high harmonic generation in liquids. *Phys. Rev. Lett.* **124**, 203901 (2020).
13. C. Yu, K. K. Hansen, L. B. Madsen, Enhanced high-order harmonic generation in donor-doped band-gap materials. *Phys. Rev. A* **99**, 013435 (2019).
14. A. Pattanayak, M. S. Mrudul, G. Dixit, Influence of vacancy defects in solid high-order harmonic generation. *Phys. Rev. A* **101**, 013404 (2020).
15. B. Brutscky, The structure of microsolvated benzene derivatives and the role of aromatic substituents. *Chem. Rev.* **100**, 3891–3920 (2000).
16. A. Alharbi *et al*., Sensitivity of high-order-harmonic generation to aromaticity. *Phys. Rev. A* **92**, 041801 (2015).
17. K. Schafer, B. Yang, L. DiMauro, K. Kulander, Above threshold ionization beyond the high harmonic cutoff. *Phys. Rev. Lett.* **70**, 1599 (1993).
18. P. B. Corkum, Plasma perspective on strong field multiphoton ionization. *Phys. Rev. Lett.* **71**, 1994 (1993).
19. L. Lagardère *et al*., Tinker-HP: A massively parallel molecular dynamics package for multiscale simulations of large complex systems with advanced point dipole polarizable force fields. *Chem. Sci.* **9**, 956–972 (2018).
20. W. L. Jorgensen, D. S. Maxwell, J. Tirado-Rives, Development and testing of the OPLS all-atom force field on conformational energetics and properties of organic liquids. *J. Am. Chem. Soc.* **118**, 11225–11236 (1996).
21. P. Jedlovszky, The local structure of various hydrogen bonded liquids: Voronoi polyhedra analysis of water, methanol, and HF. *J. Chem. Phys.* **113**, 9113–9121 (2000).
22. I. Svishchev, P. Kusalik, Structure in liquid methanol from spatial distribution functions. *J. Chem. Phys.* **100**, 5165–5171 (1994).
23. J. M. Herbert, K. Carter-Fenk, Electrostatics, charge transfer, and the nature of the halide-water hydrogen bond. *J. Phys. Chem. A* **125**, 1243–1256 (2021).
24. M. Tudorovskaya, M. Lein, High-order harmonic generation in the presence of a resonance. *Phys. Rev. A* **84**, 013430 (2011).
25. S. Chandra, I. N. Ansari, G. Dixit, F. Lepine, A. Bhattacharya, Experimental evidence of sensitivity of the high harmonic generation to hydrogen bonding. *J. Phys. Chem. A* **123**, 5144–5149 (2019).
26. J. M. Herbert, M. P. Coons, The hydrated electron. *Annu. Rev. Phys. Chem.* **68**, 447–472 (2017).
27. F. Martin *et al*., DNA strand breaks induced by 0–4 ev electrons: The role of shape resonances. *Phys. Rev. Lett.* **93**, 068101 (2004).
28. B. Sulik *et al*., Fermi-shuttle processes in the electron emission by ion impact: Contribution to radiation damages. *Radiat. Phys. Chem.* **76**, 483–486 (2007).
29. E. Alizadeh, A. G. Sanz, G. Garcia, L. Sanche, Radiation damage to DNA: The indirect effect of low-energy electrons. *J. Phys. Chem. Lett.* **4**, 820–825 (2013).
30. J. D. Koralek *et al*., Generation and characterization of ultrathin free-flowing liquid sheets. *Nat. Comm.* **9**, 1353 (2018).
31. S. Giri, 1D_tdse_model. Github. https://github.com/girisucharita/1D_tdse_model.git. Deposited 24 October 2025.